OXFORD UNIVERSITY PRESS | Carcinogenesis

Osteopontin drives KRAS-mutant lung adenocarcinoma

Journal:	*Carcinogenesis*
Manuscript ID	CARCIN-2019-00229.R1
Manuscript Type:	Original Article
Date Submitted by the Author:	15-Oct-2019
Complete List of Authors:	Giopanou, Ioanna; University of Patras School of Health Sciences, Physiology Kanellakis, Nikolaos ; University of Patras School of Health Sciences, Physiology Giannou, Anastasios; University of Patras, Faculty of Medicine Lilis, Ioannis; University of Patras School of Health Sciences, Physiology Marazioti, Antonia; University of Patras School of Health Sciences, Physiology Spella, Magda; University of Patras School of Health Sciences, Physiology Papaleonidopoulos, Vassilios; University of Patras School of Health Sciences, Physiology Simoes, Davina ; University of Northumbria at Newcastle, Department of Applied Sciences Zazara, Dimitra; University of Patras, Faculty of Medicine, Laboratory for Molecular Respiratory Carcinogenesis Agalioti, Theodora; University of Patras, Faculty of Medicine Moschos, Charalampos; National and Kapodistrian University of Athens School of Health Sciences, 1st Department of Critical Care and Pulmonary Medicine Magkouta, Sophia; National and Kapodistrian University of Athens School of Health Sciences, 1st Department of Critical Care and Pulmonary Medicine Kalomenidis, Ioannis; National and Kapodistrian University of Athens School of Health Sciences, 1st Department of Critical Care and Pulmonary Medicine Panoutsakopoulou, Vily; Biomedical Research Foundation of the Academy of Athens, Cellular Immunology Laboratory Lamort, Anne; Ludwig-Maximilians-Universitat Munchen, 5ComprehensivPneumology Center (CPC) and Institute for Lung Biology and Disease (iLBD) Stathopoulos, Georgios; University of Patras School of Health Sciences, Physiology Psallidas, Ioannis; University of Patras, Faculty of Medicine, Laboratory for Molecular Respiratory Carcinogenesis
Keywords:	SPP1; KRAS; urethane; lung cancer; survival.

Osteopontin drives *KRAS*-mutant lung adenocarcinoma

Ioanna Giopanou[1,*], Nikolaos I. Kanellakis[1],Anastasios D. Giannou[1], Ioannis Lilis[1], Antonia Marazioti[1], Magda Spella[1],Vassilios Papaleonidopoulos[1], Davina C.M. Simoes[2], Dimitra E. Zazara[1], Theodora Agalioti[1], Charalampos Moschos[3], Sophia Magkouta[3], Ioannis Kalomenidis[3], Vily Panoutsakopoulou[4,†], Anne-Sophie Lamort[5], Georgios T. Stathopoulos[1,5,8,*], and Ioannis Psallidas[1,6,7,8].

[1] *Laboratory for Molecular Respiratory Carcinogenesis, Department of Physiology; Faculty of Medicine, University of Patras; Rio, Achaia, 26504; Greece.*

[2] *Department of Applied Sciences, Faculty of Health and Life Sciences, Northumbria University Newcastle, Newcastle upon Tyne, UK.*

[3] *"Marianthi Simou Laboratory", 1st Department of Critical Care and Pulmonary Medicine, National and Kapodistrian University of Athens, School of Medicine, Evangelismos Hospital, 10675 Athens, Greece*

[4] *Cellular Immunology Laboratory, Center for Basic Research, Biomedical Research Foundation of the Academy of Athens, Athens 11527, Greece*

[5]*Comprehensive Pneumology Center (CPC) and Institute for Lung Biology and Disease (iLBD); University Hospital, Ludwig-Maximilians University and Helmholtz ZentrumMünchen, Member of the German Center for Lung Research (DZL); Munich, Bavaria, 81377; Germany.*

[6] *Oxford Centre for Respiratory Medicine, Oxford University Hospitals NHS Trust, Oxford, UK*

[7]*Lungs for Living Research Centre, UCL Respiratory, University College London, London, UK*

[8]*Co-senior authors*

† *Deceased*

*** Corresponding Authors to whom requests for reprints and correspondence should be addressed:** Ioanna Giopanou (giopanou@upatras.gr) and Georgios T. Stathopoulos (gstathop@upatras.gr), Faculty of Medicine, University of Patras; 1 Asklepiou Str., University Campus, 26504 Rio, Greece; Phone: +302610969154; Fax: +302610969176.

Abstract

Increased expression of osteopontin (SPP1) is associated with aggressive human lung adenocarcinoma, but its function remains unknown. Our aim was to determine the role of SPP1 in smoking-induced lung adenocarcinoma. We combined mouse models of tobacco carcinogen-induced lung adenocarcinoma, of deficiency of endogenous *Spp1* alleles, and of adoptive pulmonary macrophage reconstitution to map the expression of SPP1 and its receptors and determine its impact during carcinogenesis. Co-expression of *Spp1* and mutant *Kras*^{G12C} in benign cells was employed to investigate SPP1/KRAS interactions in oncogenesis. Finally, intratracheal adenovirus encoding *Cre* recombinase was delivered to *LSL.KRAS*^{G12D} mice lacking endogenous or overexpressing transgenic *Spp1* alleles. SPP1 was overexpressed in experimental and human lung adenocarcinoma and portended poor survival. In response to two different smoke carcinogens, *Spp1*-deficient mice developed fewer and smaller lung adenocarcinoma with decreased cellular survival and angiogenesis. Both lung epithelial- and macrophage-secreted SPP1 drove tumor-associated inflammation, while epithelial SPP1 promoted early tumorigenesis by fostering the survival of *KRAS*-mutated cells. Finally, loss and overexpression of *Spp1* was, respectively, protective and deleterious for mice harboring *KRAS*^{G12D}-driven LADC. Our data support that SPP1 is functionally involved in early stages of airway epithelial carcinogenesis driven by smoking and mutant *KRAS* and may present an important therapeutic target.

Running Title: Osteopontin in lung carcinogenesis.

Key words: SPP1; KRAS; urethane; lung cancer; survival.

Summary: Here we used mouse models of chemically and genetically induced lung adenocarcinoma combined with mice engineered to lack or overexpress osteopontin genes

and with human observations to identify osteopontin's exact role during lung tumor development.

Introduction

Lung cancer is the leading cancer killer, claiming 1.73 million lives and 36 million years of life lost worldwide in 2015 alone and lung adenocarcinoma (LADC) constitutes the deadliest human neoplasm *per se* [1,2]. Although 15% of LADC cases occur in never smokers, tobacco smoking is the leading risk factor for LADC [3,4]. LADC of smokers most frequently harbor mutations in the KRAS protooncogene GTPase (*KRAS*), which are notoriously undruggable. Patients with *KRAS*-mutant LADC are in need for new targeted therapies that prerequisite a deeper understanding of the pathobiology of the disease [5,6].Osteopontin (secreted phosphoprotein 1, SPP1; encoded by the human/murine *SPP1*/*Spp1* genes), is a secreted, chemokine-like, matricellular phosphoglycoprotein that is widely expressed in the human body [7]. Although SPP1 facilitates physiologic processes, it has also been shown to drive tumor progression in mouse models of different metastatic cancers [8-12]. Elevated SPP1 expression has been associated with worse lung cancer patients prognosis [13] and its knock-down inhibited the growth of lung cancer cell lines [11,14]. Importantly, deficiency in the SPP1 receptor CD44 and exogenous delivery of non-functional decoy SPP1 were protective in genetic mouse models of LADC [15,16]. However, the functional role of SPP1 in physiologically relevant mouse models of *de novo* development of LADC in response to tobacco chemicals [17,18] has not been studied.

The aim of this study was to map and investigate the functional role of SPP1, and to identify its action during *de novo* LADC development in response to tobacco carcinogens. For this, multiple mouse models of SPP1 deficiency and overexpression were deployed in combination with cellular models of survival competition. The results demonstrate the importance of SPP1 in early stages of cell-autonomous lung tumor formation and progression

and provide a direct link between *KRAS* mutations and the tumorigenic activity of SPP1, positioning SPP1 as a therapeutic target against *KRAS*-mutant LADC.

Materials and methods

Additional details can be found in the supplementary information material at http://carcin.oxfordjournals.org/.

Ethics approval: Experiments were carefully designed and preapproved by the Veterinary Administration of the Prefecture of Western Greece (approvals #3741/16.11.2010, 60291/3035/19.03.2012, and 118018/578/30.04.2014) and conducted according to Directive 2010/63/EU (http://eur-lex.europa.eu/LexUriServ/LexUriServ.do?uri= OJ:L:2010:276:0033:0079:EN:PDF).

Human data: BATTLE study microarrays were from GEO series GSE43458 [19]. *SPP1/ACTB* transcript abundance was determined for each patient using Affymetrix (Santa Clara, CA) software. Survival was analyzed on Kaplan-Meier Plotter (http://kmplot.com/analysis/; [20]) using: probe ID = 209875_s_at; auto-select best cut-off; compute median survival; histologic subtype =All or LADC; Cox regression = multivariate including AJCC stages T and N.

Cell line authedication: Human HEK293T embryonic kidney cells were a generous gift from Professor's Ioannis Kalomenidis laboratory in January 2016. Primary LADC cells were isolated from urethane-induced LADC of *FVB* mice in our laboratory as described previously [21]. All cell lines were tested biannually using short tandem repeats (STR) and *Mycoplasma Spp* PCR and were cultured at 37 ^{o}C in 5% CO2-95% air using DMEM/10% FBS/2 mM L-glutamine/1 mM pyruvate/100 U/mL penicillin/100 mg/mL streptomycin. Cells were used for experiments after 5 passages.

Vectors and cell treatments: Plasmids used ([21-24]; http://www.addgene.org/Georgios_Stathopoulos/; ID's in parentheses) include p*C* (6691 Bicistronic_ires_puro; 64335), p*Spp1* (pSpp1-is2; 58248), p*RFP* (Plenti-CMV-MCS-RFP-SV-puro; 109377; gift from Jonathan Garlick & Behzad Gerami-Naini), p*GFP* (7432 Bicistronic_GFP_ires_puro; 64336), p*GFP.Kras*^{G12C} (8027_GFP-KrasG12C_2B_puro; 64372), and p*Cag.Luc* (Cag.Luc.puro; 74409). Cells were transfected with 5 μg DNA using calcium phosphate. Stable clones were selected using puromycin (1-7 μg/mL). Cells were treated with daily recombinant murine SPP1 (rmSPP1; 40 ng/mL; #441-OP-050; R&D Systems, Minneapolis, MN) or neutralizing SPP1 antibodies (α-SPP1; 10 μg/mL; anti-mouse #ab11503, Abcam, Cambridge, MA; anti-human AF1433, R&D Systems, Minneapolis, MN).

Mouse models of LADC: *C57BL/6J* (*C57BL/6*; #000664), B6.129S6-*Spp1*^{tm1Blh}*/J (Spp1*$^{-/-}$; #004936; [25]), *FVB/NJ* (*FVB*; #001800), B6.129S4-*Kras*^{tm4Tyj}*/J* (*LSL.KRAS*^{G12D}; #008179; [26]),FVB-Tg$^{(CAG\text{-}luc,\text{-}GFP)L2G85Chco}$*/J*(*CAG-luc-eGFP*; #008450; [27]),and NOD.CB17-*Prkdc*$^{<scid>}$*/J* (*NOD/SCID*; #001303; [28]) mice from Jackson Laboratories and *Spp1-stop*$^{f/f}$*/CreER*^{T1}(*LSL.Spp1*^{Tg};[29]) mice were bred in the University of Patras Center for Animal Models of Disease (for mouse numbers see supplementary Table 1). LADC was induced in *FVB* mice using a single (*CAG-luc-eGFP* mice) or four (wild-type *FVB* mice) consecutive weekly intraperitoneal injections of 1 g/Kg urethane (CAS#51-79-6; Sigma Aldrich; St. Louis, MO) and in *C57BL/6* mice using ten weekly injections [17,22]. Alternatively, LADC was triggered in *C57BL/6* mice by four consecutive weekly intraperitoneal injections of 15 mg/Kg 3-methylcholanthrene (MCA; CAS#56-49-5; Sigma) followed by six consecutive weekly intraperitoneal injections of 200 mg/Kg butylatedhydroxytoluene (BHT; CAS#128-37-0; Sigma; [30]). Experimental mice were sex-, weight (20–25 g)-, and age (6–12 week)-matched, were initiated on treatments at 6 weeks of age, and were sacrificed 4 months (*FVB* mice), 1 or 6 months (*C57BL/6* mice), or 2 weeks

(*CAG-luc-eGFP* mice) following treatment. *KRAS*^{G12D}-driven LADC was induced via intratracheal delivery of 5 x 10^8 plaque-forming units (PFU) of adenovirus type 5 encoding CRE recombinase (Ad-*Cre*; Vector Development Lab, Baylor College of Medicine; Houston, TX) to *LSL.KRAS*^{G12D} mice [26]. For flank oncogenesis, *NOD/SCID* mice received 2 x 10^6 subcutaneous HEK293T cells and vertical tumor diameters (δ) were measured. Mice were imaged for bioluminescent detection of cell mass weekly thereafter. Cell spot volume (V) was calculated as $V = \pi \times (\delta 1 \times \delta 2 \times \delta 3)/6$. For LADC development following adoptive alveolar macrophage reconstitution, *FVB* mice received total-body irradiation (900 Rad) followed 12 hours later by 10^7 intravenous bone marrow cells obtained from the four long bones of *Spp1*$^{+/+}$ or *Spp1*$^{-/-}$ mice, one month thereafter by intratracheal clodronate (0.5 mg in 100 μL), and yet another month thereafter by four consecutive weekly intraperitoneal urethane (1 g/Kg) injections [23,31].

Imaging: For bioluminescence imaging, cells and mice were serially imaged on an Xenogen Lumina II after delivery of 300 μg/mL D-luciferin (Gold Biotechnology; St. Louis, MO) to culture media or 1 mg intravenous D-luciferin into the retroorbital veins. Data were analyzed using Living Image v.4.2 (Perkin-Elmer, Waltham, MA; [17,22,23].

Statistics: Sample size (*n*; always biological) was determined using G*power [32], assuming $\alpha = 0.05$, $\beta = 0.05$, and $d = 1.5$. Data were acquired by two blinded readers, reevaluated if >20% deviant (no data were excluded), examined for normality by Kolmogorov-Smirnov test, and presented and analyzed as appropriate. Differences in frequencies were examined by χ^2 test, in means by t-test or one-way ANOVA/Tukey's post-tests, in medians by Mann-Whitney test or Kruskal-Wallis/Dunn's post-tests, in measurements over time by two-way ANOVA/Bonferroni post-tests, and in survival by Kaplan-Meier estimates/log-rank tests and

Cox regression. Probability (P) is two-tailed and $P < 0.05$ was considered significant. Statistics and plots were done on Prism v5.0 (GraphPad, La Jolla, CA).

Results

SPP1 is overexpressed in LADC and portends poor survival

To assess SPP1 as a candidate driver of human LADC, we determined its expression in a well-defined microarray study of 30 normal lung samples and 80 LADC tissues from the BATTLE study (https://www.ncbi.nlm.nih.gov/geo/query/acc.cgi?acc=GSE43458; [19]). Raw data of each patient were analyzed separately and normalized to *ACTB* housekeeping transcripts, revealing marked overexpression of *SPP1* in LADC compared with normal lung tissue (Figure 1A). This fact was corroborated using The Human Protein Atlas (https://www.proteinatlas.org/ENSG00000118785-SPP1/pathology; [33]). In line with published studies [13,34,35], high SPP1 expression was also an unfavorable prognostic marker for 1,150 patients with lung cancer and 231 patients with LADC from the Kaplan-Meier Plotter database (Figure 1B, 1C). We next sought to map SPP1 expression in chemical-induced LADC of mice, which features a mutation profile that is highly similar to human LADC [18]. For this, *C57BL/6* mice competent ($Spp1^{+/+}$), haploinsufficient ($Spp1^{+/-}$), or deficient ($Spp1^{-/-}$) in *Spp1* alleles received ten consecutive intraperitoneal injections of urethane (1 g/Kg) and were examined for immunohistochemical detection of SPP1 immunoreactivity of lung tissues together with untreated *Spp1*-competent mice. In naïve mice, SPP1 expression was restricted to non-ciliated airway epithelial (club or Clara) cells (Figure 1D). In tumor-bearing lungs of *Spp1*-competent mice, SPP1 was highly and ubiquitously overexpressed in lung tumors, airway and alveolar epithelial cells, and alveolar macrophages; no SPP1 immunoreactivity was evident in the lungs from *Spp1*-deficient mice or when primary antibody was omitted (Figure 1E). A time-course experiment examining

SPP1 protein levels in bronchoalveolar lavage (BAL) from urethane-treated *Spp1*$^{+/+}$, *Spp1*$^{+/-}$, and *Spp1*$^{-/-}$ mice by ELISA corroborated the progressively increasing release of SPP1 into the airspaces of urethane-treated *Spp1*$^{+/+}$ mice and validated SPP1 deficiency of both *Spp1*$^{+/-}$ and *Spp1*$^{-/-}$ mice (Figure 1F). Similar results were obtained when RNA extracted from LADC cells isolated from urethane-induced lung tumors [21,24], from lungs of naïve mice, and from lungs of urethane-treated mice (one week latency) was analyzed by microarray and qPCR. These analyses corroborated the overexpression of *Spp1*, and also identified *Itgav*, *Itgb1*, *Itgb3*, *Itgb5*, and *Cd44* as the main SPP1 receptors overexpressed by LADC cells relative to *Gusb* housekeeping transcript (Figure 1G, 1H). The ITGB3 protein overexpression by LADC cells was also evident by immunofluorescence (Figure 1I). Collectively, these findings supported that SPP1 signaling may be important in LADC biology and warranted further investigation.

SPP1 promotes chemical-induced LADC in mice

To define the impact of SPP1 in LADC, we exposed *Spp1*$^{+/+}$, *Spp1*$^{+/-}$, and *Spp1*$^{-/-}$mice (*C57BL/6*) to ten repetitive urethane treatments and waited six months in order to generate chemical-induced LADC with *Kras* mutations [22]. As shown in Figure 2A-2F, *Spp1*$^{-/-}$ mice were markedly resistant to lung tumor induction compared with *Spp1*$^{+/+}$ mice, and *Spp1*$^{+/-}$ mice showed a phenotype closely resembling *Spp1*$^{-/-}$ mice, in line with their almost complete SPP1 protein deficiency in BAL (Figure 1F). *Spp1*$^{+/+}$ and *Spp1*$^{-/-}$ mice were also exposed to a second two-hit chemical carcinogen model of repetitive MCA-BHT injections, with similar results indicating marked resistance of *Spp1*-gene-deficient mice to chemical lung tumor induction (Figure 2G-2L). To identify how SPP1 functions as tumor promoter, we further studied parameters of inflammation, cellular proliferation, apoptosis, and angiogenesis in the lungs of mice. To this end, *Spp1*$^{-/-}$ mice had fewer inflammatory cells in BAL, more PCNA+

and TUNEL+ cells in lung tumors, and fewer F8A+ angiogenic hotspots in lung tumors compared with *Spp1*$^{+/+}$ mice (Figure 3). The decreased proliferation/apoptosis ratio of lung tumors from *Spp1*$^{-/-}$ mice (determined as the ratio of PCNA+ dividing to TUNEL+ apoptotic cells) indicated that the enhanced cell proliferation observed was a rebound effect caused by the massive apoptotic rates they displayed (Figure 3G). Taken together, these results show that SPP1 promotes carcinogen-induced inflammation, cell proliferation, and angiogenesis, culminating in net tumor promotion at late stages post-carcinogen exposure.

Epithelial-derived SPP1 fosters cellular proliferation in the preneoplastic lung

The multifaceted phenotype of tumor-bearing *Spp1*$^{-/-}$ mice could be attributed to decreased epithelial proliferation at early stages of carcinogenesis leading to less progressed tumors causing less inflammation and angiogenesis (cell-autonomous effects of epithelial SPP1), or to tumor-promoting effects of tumor-infiltrating immune cells during late stages of carcinogenesis (paracrine effects of myeloid SPP1). To determine the mechanism, we performed two experiments. First, *Spp1*$^{+/+}$, *Spp1*$^{+/-}$, and *Spp1*$^{-/-}$mice (*C57BL/6*) received four repetitive urethane treatments and were sacrificed prematurely thereafter (Figure 4A). In this model of early lung carcinogenesis [36], *Spp1*$^{-/-}$ mice displayed decreased inflammatory cells in BAL, fewer alveolar hyperplastic lesions, and statistically significantly fewer proliferating cells in hyperplastic lesions and airway epithelium (Figure 4B-4F). In a second experiment aimed at dissecting epithelial- versus myeloid-SPP1 effects, wild type FVB mice were subjected to total-body irradiation (900 Rad) followed by adoptive bone marrow transfer of ten million whole bone marrow cells obtained from *Spp1*$^{+/+}$ and *Spp1*$^{-/-}$ donors [23,24]. One month later, when the native bone marrow was fully reconstituted by the transplants, all chimeric mice received intratracheal clodronate dosed to kill their alveolar macrophages, a technique previously shown to efficiently repopulate the lungs with bone marrow-derived

macrophages [31].Yet another month thereafter, all animals with *Spp1*-competent lung epithelium and either *Spp1*-competent or -deficient lung myeloid cells were exposed to four consecutive urethane injections according to an accelerated tumorigenesis protocol (Figure 4G; [17]). Lung examination revealed no differences in tumor incidence, multiplicity, or size between chimeric mice with *Spp1*$^{+/+}$ and *Spp1*$^{-/-}$ alveolar macrophages (achieved power 91%) but showed that the latter mice exhibited statistically significantly decreased numbers of BAL inflammatory cells (Figue 4h-4l). This experiment showed that epithelial-derived SPP1 drives chemical-induced LADC, while both epithelial- and myeloid-derived SPP1 drive tumor-associated inflammation, consistent with results from transplantable cancer models [10,11]. Collectively, the results indicate that epithelial-expressed SPP1 has a significant role in the establishment of clusters of proliferating cells with tumorigenic characteristics at early stages of lung carcinogenesis.

SPP1 drives the survival of *KRAS*-mutant cells

Since chemical-induced lung tumors of mice are *Kras*-mutant [18,22], and based on the above results that supported cell-autonomous effects of epithelial SPP1, we sought to test the impact of SPP1 on cell proliferation in the cellular contexts of wild-type versus mutant *Kras*. For this reason we decided to use HEK293T embryonic kidney cells, a cell line that is easily tranfected and does not bear mutant *Kras* or any syngeneic mutations in the *Egfr-Kras* pathway in order to have an insight into a more close to human approach. We first optimized transient transfection protocols of HEK293T cells with a p*GFP* eukaryotic expression vector, obtaining >90% transfection efficiency using >10 ng DNA/2 x 10^4 cells at 96 hours (Figure 5A, 5B). HEK293T cells were subsequently stably transfected with p*GFP* or p*RFP*, followed by transient transfection with vectors encoding mutant murine *Kras*^{G12C}and/or murine SPP1, mixing of equal numbers of p*GFP* (test) and p*RFP* (control)-expressing cells, and co-culture

for one week in *in vitro* competition assays. Alternatively, co-incubation for one week with rmSPP1 or anti-human α-SPP1 was performed. Quantification of p*GFP*+ and p*RFP*+ cells by fluorescent microscopy and flow cytometry revealed that forced overexpression of pΔ*Kras* alone impaired the survival of HEK293T cells, similar to our previous results with other cell lines [21]. This pΔ*Kras*-induced anti-survival effect was completely preventable by p*Spp1* overexpression and by co-incubation with exogenous rmSPP1 and was further aggravated by co-incubation with α-SPP1 (Figure 5C-5E). In a second experimental approach, *CAG-luc-eGFP* mice constitutively expressing *Photinus pyralis* luciferase in all somatic cells ([27]; *FVB* strain) received a single intraperitoneal injection of urethane (1 g/Kg), were sacrificed after two weeks (when *Kras* mutations occur in the lungs; [37], and single cell suspensions of pulmonary cells (50 000 cells/mouse) were incubated for two weeks with PBS control, rmSPP1, or anti-mouse α-SPP1. Bioluminescent detection of cell mass and cell counting revealed that exogenous rmSPP1 fostered and neutralization of endogenous SPP1 using α-SPP1 inhibited the survival of tumor-initiated pulmonary cells (Figure 5F-5H). These results suggested that epithelial-derived SPP1 potentially selectively sustains the survival of *Kras*-mutant epithelial cells in an autocrine and/or paracrine fashion. To definitively test this, we stably transfected HEK293T cells with a vector encoding *Photinus pyralis* luciferase (p*Cag.Luc*) with or without p*ΔKras*, followed by transient transfections with a control (p*C*) or p*Spp1* vectors. Upon validation, 2 x 10^6 transfected cells were injected pairwise into the rear flanks of *NOD/SCID* mice followed by serial tumor measurements and bioluminescence imaging. As shown in Figure 6, pΔ*Kras* or p*Spp1* alone did not render HEK293T cells tumorigenic, but simultaneous overexpression of pΔ*Kras* and p*Spp1* resulted in formation of large primary tumors in 50% of the mice injected. These data corroborated that SPP1 can function as a promoter of *Kras*-mutant tumors *in vivo*.

SPP1 is required for *KRAS*^{G12D}-driven LADC

To further prove the pro-tumor effects of SPP1 on KRAS-mutant tumors, we generated intercrosses of mice conditionally expressing mutant *KRAS*^{G12D} upon CRE-mediated recombination (*LSL.KRAS*^{G12D}; [26]) with *Spp1*$^{+/+}$, *Spp1*$^{+/-}$, and *Spp1*$^{-/-}$ mice. The transgenic mice received intratracheally Ad-*Cre* and were sacrificed 4 months later. Similar to results from chemical models, *Spp1* gene-deficiency was protective from *KRAS*^{G12D}-driven LADC (Figure 6H, 6K). To strengthen our findings using additional models, but also to highlight the possible autocrine effects of SPP1, *LSL.KRAS*^{G12D} mice were intercrossed with mice conditionally overexpressing SPP1 upon CRE-mediated recombination (*LSL.SPP1*^{Tg}, [29]) and offsprings received 5 x 10^8 PFU Ad-*Cre* and were sacrificed 3 months later. In this model, oncogenic *KRAS*^{G12D} and SPP1 were co-expressed sporadically in the respiratory epithelium. Again, SPP1 overexpression specifically in *KRAS*^{G12D}-initiated cells (see Supplementary Figure 2) markedly enhanced carcinogenesis (Figure 6J, and 6L), solidifying the link between SPP1 and mutant *KRAS*.

Discussion

In the present study, we investigated the functional role of SPP1 in autochthonous airway epithelial carcinogenesis induced by two different tobacco chemicals and by oncogenic mutant *KRAS*^{G12D}. In accord with previous studies, analyses of multiple published datasets confirmed the marked (>25-fold) overexpression of SPP1 in LADC compared with adjacent non-tumorous lung tissues, as well as its importance in predicting poor survival [13,38-40]. Our findings are the first to demonstrate that SPP1 is overexpressed and required for murine LADC induction by two different tobacco carcinogens. Collectively, the data presented support that lung epithelial SPP1 sustains the survival of *KRAS*-mutant lung epithelial cells at early time points post-carcinogen exposure, while myeloid-secreted SPP1 drives tumor-

associated inflammation. Finally, an unequivocal role for SPP1 as a tumor promoter in the cellular context of mutant *KRAS* is shown using xenotransplant models and mouse models of stochastic *KRAS* mutation infliction in the murine respiratory epithelium.

Epithelial SPP1 is shown here to function in a cell-autonomous fashion to drive the survival of *KRAS*-mutated lung epithelial cells. This is supported by the decreased cellular proliferation and the increased apoptosis of epithelial cells in the lungs of *Spp1*-gene-deficient mice upon carcinogen exposure, by the survival advantage of cells co-expressing mutant *KRAS* and SPP1 *in vitro* and *in vivo*, and by the results from genetic models where $KRAS^{G12D}$ and SPP1 expression were stochastically inflicted in the same cells across the lung epithelium. This mechanism of SPP1 effects in LADC is plausible, since pulmonary tumor initiated cells expressed at the same time SPP1 and a battery of its receptors' transcripts, including *Itgav*, *Itgb1*, *Itgb3*, *Itgb5*, and *Cd44*. In particular integrinβ3 (ITGB3), which was validated at the protein level to be focally expressed by the respiratory epithelium and lung tumors in our chemical models, was recently shown to drive lung tumor cell stemness and drug resistance by interacting with oncogenic *KRAS* to promote non-canonical activation of nuclear factor (NF)-κB [41]. Hence SPP1 and ITGB3 signaling might be the missing link between *KRAS* mutations and alternative NF-κB pathway activation that we recently reported in patients and mice with LADC [17,22,23,42]. Our results are also in line with the role of SPP1 in causing the radiation resistance of *KRAS*-mutated lung cancers [43] and with the effects of CD44, another SPP1 receptor, in driving *KRAS*-mutant lung cancers [15,44]. Taken together, our results explain previous links of SPP1 to enhanced lung cancer progression and pin the cytokine's pro-tumor functions to a defined molecular subclass of this cancer type, i.e.*KRAS*-mutant lung adenocarcinomas of smokers.

One of the most interesting findings from adoptive bone marrow transplant experiments was that selectively SPP1 of epithelial origin fuels chemical-induced LADC development, while myeloid-derived SPP1 participates in mounting tumor-associated inflammation without impacting carcinogenesis. The latter observation does not provide experimental support to a report of increased macrophage SPP1 expression in lung cancer patients, which was correlated with poor survival [39]. Notwithstanding a potential tumor-promoting effect of immune-derived SPP1 in lung cancer not evident in the bone marrow transplant model employed here, our studies highlight the prime mechanism of the pro-tumorigenic functions of SPP1 in the lungs: SPP1 expressed by the tumor-initiated pulmonary epithelium promotes the survival of transformed cells that harbor *KRAS* mutations. To this end, recent and earlier studies in patients with lung cancer have underlined SPP1 as a peripheral blood biomarker of disease progression and response to therapy [38-40,45,46] and their findings can be explained by the tissue-restricted effects of epithelial SPP1 reported here. The latter can be explained by different isoforms of SPP1 potentially secreted by epithelial and myeloid cells, as well as the differential effects of the cytokine depending on cellular *TP53* mutation status [11]. The known facts that mature chemical-induced LADC commonly carry deleted or mutated *Trp53* alleles [18,47], and that SPP1 functions to promote cellular survival especially in the cellular context of functional, wild-type *TP53* alleles [11], further supports our findings of early effects of SPP1 post-carcinogen exposure.

Our findings have explicit clinical implications and we hope that they will prompt clinical progress aimed at inhibiting SPP1 in lung cancer, in addition to using it as a biomarker of tumor mass, survival, and therapy response [38,39,45]. Despite potential therapeutic applications in patients with established malignant lung tumors, we believe that the major potential clinical application of our findings would be SPP1-targeted chemoprevention strategies to prevent LADC development in smokers. This is feasible given the multitude of

the agents available to inhibit SPP1 signaling [16,29,45]. The concept of lung cancer chemoprevention targeted at tumor-associated inflammation is an emerging certainty in the field after the results of the Canakinumab Anti-inflammatory Thrombosis Outcomes Study (CANTOS) trial: neutralization of interleukin-1β using the humanized monoclonal antibody canakinumab aimed at reduction of cardiovascular risk achieved its primary endpoint by decreasing cardiovascular events by up to 15% [48], at the same time inadvertently decreasing lung cancer mortality in the high-dose intervention group by an astonishing 77% [49]. We believe that SPP1 could be an equally lucrative target for chemoprevention of incident LADC in ever smokers at high risk for the disease. In conclusion, osteopontin is shown to play a pivotal tumor promoting role in early stages of lung adenocarcinoma development. Evidence from multiple mouse models and from humans is presented that pins the cytokine as a prime target for chemoprevention of lung adenocarcinoma in the lungs of smokers.

Authors' contributions

IG performed *in vivo* experiments, histology, and wrote the first draft of the manuscript; NIK did microarrays and qPCR; IL did immunohistochemistry and morphometry; VP performed *in vitro* GFP-reporter assays; DMS generated/contributed SPP1-deleted mice; ADG, CM, AM, SM, IK performed *in vivo* experiments, VP contributed conditional SPP1-overexpressing mice; ASL analyzed human survival/ microarray data; DEZ performed immunofluorescence; TA generated eukaryotic expression vectors; GTS analyzed all data and created the figures; GTS and PI designed, wrote the final version of the manuscript, and are the guarantors of the study's integrity. All authors critically reviewed the paper for important intellectual content and approved the final submitted version.

Conflict of Interest Statement

The authors declare no conflict of interest.

Funding

This work was supported by the European Research Council 2010 Starting Independent Investigator and 2015 Proof of Concept Grants (260524 and 679345, respectively, to GTS). I.G. is a recipient of a Greek State Scholarship Foundation (IKY) programme co-financed by the European Union (European Social Fund-ESF), by Greek national funds through an action entitled "Reinforcement of Postdoctoral Researchers" (NSRF 2014 – 2020). I. Psallidas is the recipient of a REPSIRE2 European Respiratory Society Fellowship (grant number 2015–7160).

References

1. Fitzmaurice, C., *et al.* (2017) Global, Regional, and National Cancer Incidence, Mortality, Years of Life Lost, Years Lived With Disability, and Disability-Adjusted Life-years for 32 Cancer Groups, 1990 to 2015: A Systematic Analysis for the Global Burden of Disease Study. *JAMA Oncol*, **3**, 524-548.

2. (2014) Comprehensive molecular profiling of lung adenocarcinoma. *Nature*, **511**, 543-50.

3. Bender, E. (2014) Epidemiology: The dominant malignancy. *Nature*, **513**, S2-3.

4. Alberg, A.J., *et al.* (2007) Epidemiology of lung cancer: ACCP evidence-based clinical practice guidelines (2nd edition). *Chest*, **132**, 29S-55S.

5. Stephen, A.G., *et al.* (2014) Dragging ras back in the ring. *Cancer Cell*, **25**, 272-81.

6. Nadal, E., *et al.* (2014) KRAS-G12C mutation is associated with poor outcome in surgically resected lung adenocarcinoma. *J Thorac Oncol*, **9**, 1513-22.

7. Ashkar, S., *et al.* (2000) Eta-1 (osteopontin): an early component of type-1 (cell-mediated) immunity. *Science*, **287**, 860-4.

8. Yin, M., *et al.* (2014) Osteopontin promotes the invasive growth of melanoma cells by activating integrin alphavbeta3 and down-regulating tetraspanin CD9. *Am J Pathol*, **184**, 842-58.

9. Sangaletti, S., *et al.* (2014) Osteopontin shapes immunosuppression in the metastatic niche. *Cancer Res*, **74**, 4706-19.

10. Psallidas, I., *et al.* (2013) Secreted phosphoprotein-1 directly provokes vascular leakage to foster malignant pleural effusion. *Oncogene*, **32**, 528-35.

11. Giopanou, I., *et al.* (2017) Tumor-derived osteopontin isoforms cooperate with TRP53 and CCL2 to promote lung metastasis. *Oncoimmunology*, **6**, e1256528.

12. Khodavirdi, A.C., *et al.* (2006) Increased expression of osteopontin contributes to the progression of prostate cancer. *Cancer Res*, **66**, 883-8.

13. Shi, S.M., *et al.* (2016) Increased osteopontin protein expression may be correlated with poor prognosis in non-small-cell lung cancer: A meta analysis. *J Cancer Res Ther*, **12**, 277-82.

14. Sun, B.S., *et al.* (2013) Osteopontin knockdown suppresses non-small cell lung cancer cell invasion and metastasis. *Chin Med J (Engl)*, **126**, 1683-8.

15. Zhao, P., *et al.* (2013) CD44 promotes Kras-dependent lung adenocarcinoma. *Oncogene*, **32**, 5186-90.

16. Minai-Tehrani, A., *et al.* (2013) Aerosol delivery of lentivirus-mediated O-glycosylation mutant osteopontin suppresses lung tumorigenesis in K-ras (LA1) mice. *Cell Oncol (Dordr)*, **36**, 15-26.

17. Stathopoulos, G.T., *et al.* (2007) Epithelial NF-kappaB activation promotes urethane-induced lung carcinogenesis. *Proc Natl Acad Sci U S A*, **104**, 18514-9.

18. Westcott, P.M., *et al.* (2015) The mutational landscapes of genetic and chemical models of Kras-driven lung cancer. *Nature*, **517**, 489-92.

19. Kabbout, M., *et al.* (2013) ETS2 mediated tumor suppressive function and MET oncogene inhibition in human non-small cell lung cancer. *Clin Cancer Res*, **19**, 3383-95.

20. Gyorffy, B., *et al.* (2013) Online survival analysis software to assess the prognostic value of biomarkers using transcriptomic data in non-small-cell lung cancer. *PLoS One*, **8**, e82241.

21. Agalioti, T., *et al.* (2017) Mutant KRAS promotes malignant pleural effusion formation. *Nat Commun*, **8**, 15205.

22. Vreka, M., *et al.* (2018) IkappaB Kinase alpha Is Required for Development and Progression of KRAS-Mutant Lung Adenocarcinoma. *Cancer Res*, **78**, 2939-2951.

23. Marazioti, A., *et al.* (2018) Myeloid-derived interleukin-1beta drives oncogenic KRAS-NF-kappaBeta addiction in malignant pleural effusion. *Nat Commun*, **9**, 672.

24. Giannou, A.D., *et al.* (2017) NRAS destines tumor cells to the lungs. *EMBO Mol Med*, **9**, 672-686.

25. Liaw, L., *et al.* (1998) Altered wound healing in mice lacking a functional osteopontin gene (spp1). *J Clin Invest*, **101**, 1468-78.

26. Jackson, E.L., *et al.* (2001) Analysis of lung tumor initiation and progression using conditional expression of oncogenic K-ras. *Genes Dev*, **15**, 3243-8.

27. Safran, M., *et al.* (2003) Mouse reporter strain for noninvasive bioluminescent imaging of cells that have undergone Cre-mediated recombination. *Mol Imaging*, **2**, 297-302.

28. Blunt, T., *et al.* (1995) Defective DNA-dependent protein kinase activity is linked to V(D)J recombination and DNA repair defects associated with the murine scid mutation. *Cell*, **80**, 813-23.

29. Kourepini, E., *et al.* (2014) Osteopontin expression by CD103- dendritic cells drives intestinal inflammation. *Proc Natl Acad Sci U S A*, **111**, E856-65.

30. Zaynagetdinov, R., *et al.* (2012) Epithelial nuclear factor-kappaB signaling promotes lung carcinogenesis via recruitment of regulatory T lymphocytes. *Oncogene*, **31**, 3164-76.

31. Everhart, M.B., *et al.* (2005) Intratracheal administration of liposomal clodronate accelerates alveolar macrophage reconstitution following fetal liver transplantation. *J Leukoc Biol*, **77**, 173-80.

32. Faul, F., *et al.* (2007) G*Power 3: a flexible statistical power analysis program for the social, behavioral, and biomedical sciences. *Behav Res Methods*, **39**, 175-91.

33. Uhlen, M., *et al.* (2017) A pathology atlas of the human cancer transcriptome. *Science*, **357**.

34. Rud, A.K., *et al.* (2013) Osteopontin is a prognostic biomarker in non-small cell lung cancer. *BMC Cancer*, **13**, 540.

35. Hu, Z., *et al.* (2005) Overexpression of osteopontin is associated with more aggressive phenotypes in human non-small cell lung cancer. *Clin Cancer Res*, **11**, 4646-52.

36. Karabela, S.P., *et al.* (2011) Neutralization of tumor necrosis factor bioactivity ameliorates urethane-induced pulmonary oncogenesis in mice. *Neoplasia*, **13**, 1143-51.

37. Ichikawa, T., *et al.* (1996) The activation of K-ras gene at an early stage of lung tumorigenesis in mice. *Cancer Lett*, **107**, 165-70.

38. Blasberg, J.D., *et al.* (2010) Reduction of elevated plasma osteopontin levels with resection of non-small-cell lung cancer. *J Clin Oncol*, **28**, 936-41.

39. Yan, C.H., *et al.* (2015) Osteopontin is a novel prognostic biomarker in early-stage non-small cell lung cancer after surgical resection. *J Cancer Res Clin Oncol*, **141**, 1371-8.

40. Ouyang, X., *et al.* (2018) Osteopontin promotes cancer cell drug resistance, invasion, and lactate production and is associated with poor outcome of patients with advanced non-small-cell lung cancer. *Onco Targets Ther*, **11**, 5933-5941.

41. Seguin, L., *et al.* (2014) An integrin beta(3)-KRAS-RalB complex drives tumour stemness and resistance to EGFR inhibition. *Nat Cell Biol*, **16**, 457-68.

42. Giopanou, I., *et al.* (2015) Comprehensive Evaluation of Nuclear Factor-kappaBeta Expression Patterns in Non-Small Cell Lung Cancer. *PLoS ONE*, **10**, e0132527.

43. Wang, M., *et al.* (2017) Radiation Resistance in KRAS-Mutated Lung Cancer Is Enabled by Stem-like Properties Mediated by an Osteopontin-EGFR Pathway. *Cancer Res*, **77**, 2018-2028.

44. Talekar, M., *et al.* (2016) Combination wt-p53 and MicroRNA-125b Transfection in a Genetically Engineered Lung Cancer Model Using Dual CD44/EGFR-targeting Nanoparticles. *Mol Ther*, **24**, 759-69.

45. Mack, P.C., *et al.* (2008) Lower osteopontin plasma levels are associated with superior outcomes in advanced non-small-cell lung cancer patients receiving platinum-based chemotherapy: SWOG Study S0003. *J Clin Oncol*, **26**, 4771-6.

46. Li, Y., *et al.* (2015) Osteopontin-expressing macrophages in non-small cell lung cancer predict survival. *Ann Thorac Surg*, **99**, 1140-8.

47. Gao, W., *et al.* (2017) KRAS and TP53 mutations in bronchoscopy samples from former lung cancer patients. *Mol Carcinog*, **56**, 381-388.

48. Ridker, P.M., *et al.* (2017) Effect of interleukin-1beta inhibition with canakinumab on incident lung cancer in patients with atherosclerosis: exploratory results from a randomised, double-blind, placebo-controlled trial. *Lancet*, **390**, 1833-1842.

49. Ridker, P.M., *et al.* (2017) Antiinflammatory Therapy with Canakinumab for Atherosclerotic Disease. *N Engl J Med*, **377**, 1119-1131.

50. Nikitin, A.Y., *et al.* (2004) Classification of proliferative pulmonary lesions of the mouse: recommendations of the mouse models of human cancers consortium. *Cancer Res*, **64**, 2307-16.

Figure Legends

Figure 1. ***Secreted phosphoprotein 1 (SPP1) is overexpressed in human and murine lung tumors and is associated with poor survival.*** (A) *SPP1* corrected for housekeeping *ACTB* transcript abundance using the -*Δ*CT method on microarray data from 30 normal lung and 80 lung adenocarcinoma (LADC) samples from the BATTLE study (GSE43458;[19]). *Circles*, data points; *lines*, median; *boxes*, interquartile range; *bars*, 50% outer quartiles; *n*, sample size; *P*, Mann-Whitney U-test probability. (B, C) Kaplan-Meier and Cox proportional hazards overall survival (OS) analyses of 1150 patients with lung cancer (B) and 231 patients with LADC (C) stratified into low (black) and high (red) *SPP1* transcript expression by optimal cut-offs shows that *SPP1* overexpression is a stage-independent negative predictor of OS. *Lines and numbers*, Kaplan-Meier survival plots and risk estimates; *P* and *HR*, Univariate Kaplan-Meier and multivariate Cox-regression probabilities (*P*) and hazard ratios (HR) with 95% confidence intervals (CI); T and N, TNM7 primary tumor and lymph node stage. (D, E) Immunodetection of SPP1 protein (brown) in lungs from naïve *C57BL/6* mice ($n = 5$; d) and from urethane-treated (ten weekly intraperitoneal injections of 1 g/kg; latency 6 months) *C57BL/6* mice competent ($Spp1^{+/+}$; $n = 23$) or deficient ($Spp1^{-/-}$; $n = 19$) in both *Spp1* alleles (E) shows high expression by non-ciliated airway epithelial cells (red arrows), alveolar epithelial cells (magenta arrows), alveolar macrophages (blue arrows), and lung tumor cells (yellow arrows) selectively from $Spp1^{+/+}$ mice. *Inlays*, isotype controls. (F) Bronchoalveolar lavage (BAL) SPP1 protein levels from urethane-treated *C57BL/6* mice competent ($Spp1^{+/+}$), haploinsufficient ($Spp1^{+/-}$), or deficient ($Spp1^{-/-}$) in *Spp1* alleles at 0 ($n = 5$/group), 1 ($n = 7$-9/group), and 6 ($n = 5$-8/group) months post-treatment start shows increased SPP1 elaboration into the airspaces during chemical carcinogenesis. *Dots*, mean; *bars*, SD; *n*, sample size; *P*, 2-way ANOVA probability; ***, $P < 0.001$ for $Spp1^{+/+}$ mice at indicated time-points compared with time-point 0 months. (G, H) Microarray (G) and qPCR (h) results of

relative abundance of SPP1 and its receptors' transcripts in RNA extracted from naïve *FVB* mouse lungs, urethane-exposed *FVB* mouse lungs at 1 week post 1 g/Kg urethane, and primary LADC cells derived from urethane-induced lung tumors ([22]; GSE94981; g, *n*= 2/group; h, *n* = 3/group) identify and validate overexpression of *Spp1*, *Itgav*, *Itgb1*, *Itgb3*, *Itgb5*, and *Cd44* (grey area) by LADC cells relative to *Gusb* housekeeping transcript. *Dots*, mean; *bars*, SD; *n*, sample size; *P*, 2-way ANOVA probability. (I) Representative integrin-β3 (ITGB3) immunoreactivity (green) of naïve murine lungs and primary LADC cells derived from urethane-induced lung tumors (*n* = 5/group) counterstained with Hoechst 33258 (blue).

Figure 2. ***SPP1 promotes chemical-induced lung carcinogenesis.*** (A-F) *Spp1*$^{+/+}$, *Spp1*$^{+/-}$, and *Spp1*$^{-/-}$ mice on the *C57BL/6* background were treated with urethane and were sacrificed six months post-urethane start for assessment of pulmonary oncogenesis. Shown are experimental schematic with each box representing one month (A), photographs of representative lungs with tumors (B, arrows), as well as data summary of mouse numbers (n) and tumor incidence (C), number of lung tumors (D), diameter of lung tumors (E), and histologic distribution of neoplastic lesions (F). *n*, sample size; *circles*, data points; *lines*, median; *boxes*, interquartile range; *bars*, 50% outer quartiles; *P*, overall probability by χ^2 test (c), Kruskal-Wallis test (D, E), and two-way ANOVA (F); * and ***, $P< 0.05$ and $P< 0.001$, respectively, for comparison of the indicated group with *Spp1*$^{+/+}$ mice by Fischer's exact test (C), Dunn's multiple comparison test (D, E), and Bonferroni post-test (F). (G-L) *Spp1*$^{+/+}$ and *Spp1*$^{-/-}$ mice on the *C57BL/6* background were treated with 3-methylcholanthrene (MCA) followed by butylated hydroxytoluene (BHT) and were sacrificed six months post-MCA start for assessment of pulmonary oncogenesis. Shown are experimental schematic with each box representing one month (G), photographs of representative lungs with tumors (H, arrows), as well as data summary of mouse numbers (n) and tumor incidence (I), number of lung tumors (J), diameter of lung tumors (K), and histologic distribution of neoplastic lesions (L)

according to [50]. *n*, sample size; *circles*, data points; *lines*, median; *boxes*, interquartile range; *bars*, 50% outer quartiles; *P*, overall probability by χ^2 test (I), Mann-Witney U-test (J, K), and two-way ANOVA (L); **, $P< 0.01$ for comparison of the indicated group with *Spp1*$^{+/+}$ mice by Bonferroni post-test (L).

Figure 3. ***SPP1 fosters inflammation, neovascularization, and cancer cell survival in de novo lung tumors.*** *Spp1*$^{+/+}$, *Spp1*$^{+/-}$, and *Spp1*$^{-/-}$ mice on the *C57BL/6* background were treated with urethane or 3-methylcholanthrene (MCA) followed by butylated hydroxytoluene (BHT) and were sacrificed six months post-treatment start as in Figures 2A and 2G, respectively. (A) Legend to experimental groups. Nucleated cell numbers of bronchoalveolar lavage (n = 16, 12, and 25, respectively, for *Spp1*$^{+/+}$, *Spp1*$^{+/-}$, and *Spp1*$^{-/-}$ mice treated with urethane (B) and n = 6/group for *Spp1*$^{+/+}$ and *Spp1*$^{-/-}$ mice treated with MCA/BHT, (C). Shown are representative images (D) from the immunoreactivity (brown color; arrows) of lung tumors from urethane-treated mice for proliferating cell nuclear antigen (PCNA, top), terminal deoxynucleotidyl nick-end labeling (TUNEL, middle), and factor VIII-related antigen (F8A, bottom) protein expression (blue color indicates hematoxylin counterstain), and data summary (E-G) from n = 7 mice/group (ten different tumors from each mouse were examined and averaged). *Inlays*, isotype controls. *n*, sample size; *circles*, data points; *lines*, median; *boxes*, interquartile range; *bars*, 50% outer quartiles; *P*, overall probability, Unpaired t-test (C) and one-way ANOVA with Tuckey's Multiple Comparison Test (B,E-G); *, $P< 0.05$, **, $P< 0.01$ and ***and $P< 0.001$, respectively, for comparison of the indicated group with *Spp1*$^{+/+}$ mice by Dunn's multiple comparison test.

Figure 4. ***Epithelial-derived SPP1 drives preneoplasia in the tumor-initiated lung.*** (A-F) *Spp1*$^{+/+}$(n = 9), *Spp1*$^{+/-}$(n = 9), and *Spp1*$^{-/-}$(n = 7) mice on the *C57BL/6* background were treated with urethane and were sacrificed one month post-treatment start. Shown are

experimental schematic with each box representing one month (A), data summary of nucleated cell numbers of bronchoalveolar lavage (B), number of atypical alveolar hyperplastic lesions (C), proliferating cell nuclear antigen (PCNA) immunoreactive cell abundance within these lesions (D), and PCNA immunoreactive cell abundance in airway epithelium (E), as well as representative images of PCNA immunoreactivity of alveolar (top) and airway (bottom) regions (F). *Inlays*, isotype controls. *n*, sample size; *circles*, data points; *lines*, median; *boxes*, interquartile range; *bars*, 50% outer quartiles; *P*, overall probability by Kruskal-Wallis test; * and ***, $P< 0.05$ and $P< 0.001$, respectively, for comparison of the indicated group with *Spp1*$^{+/+}$ mice by Dunn's multiple comparison test. (G-L) *FVB* mice received total body irradiation (900 Rad, IR) followed by same-day bone marrow transplants (ten million cells flushed from the four long bones; BMT) from *Spp1*$^{+/+}$ and *Spp1*$^{-/-}$ mice. After one month necessary for bone marrow reconstitution, chimeras received intratracheal clodronate aimed at alveolar macrophage depletion and their reconstitution by bone marrow-derived chimeric macrophages, which is complete after another month [31], when animals received urethane and were sacrificed six months post-urethane start for assessment of pulmonary oncogenesis. Shown are experimental schematic with each box representing one month (G), photographs of representative lungs with tumors (H, arrows), as well as data summary of mouse numbers (n) and tumor incidence (I), number of lung tumors (J), diameter of lung tumors (K), and nucleated cell numbers of bronchoalveolar lavage (L). *n*, sample size; *circles*, data points; *lines*, median; *boxes*, interquartile range; *bars*, 50% outer quartiles; *P*, overall probability by χ^2 test (I) and Mann-Witney U-test (J-L).

Figure 5. ***SPP1 fosters the survival of KRAS-mutant cells.*** (A, B) HEK293T benign human embryonic kidney cells were transiently transfected with varying amounts of a eukaryotic expression vector encoding enhanced GFP and green fluorescence was quantified by serial biofluorescence imaging of live cells. Shown are representative biofluorescence images (A)

and summary of data from *n* = 3 independent experiments (B). *Circles*, mean; *bars*, SD; *n*, sample size; *P*, 2-way ANOVA probability; ***, *P*< 0.001 for plasmid amounts ≥ 10 ng/well at 96 hours compared with all other time-points and with 0 ng/well DNA. (C-E) HEK293T cells were stably transfected with eukaryotic expression vectors encoding enhanced GFP (p*GFP*) or RFP (p*RFP*). Thereafter, p*GFP*-expressing cells were transiently transfected with eukaryotic expression vectors encoding mutant murine *Kras*(p*ΔKras*) alone or p*ΔKras* plus murine SPP1 (p*Spp1*), were mixed with equal numbers of p*RFP*-expressing HEK293T cells, co-cultured for one week, and finally were quantified by fluorescent microscopy and flow cytometry. Alternatively, p*RFP*-expressing cells were transiently transfected with p*ΔKras*, mixed with equal numbers of p*GFP*-expressing cells, and were co-incubated for one week with recombinant murine SPP1 (rmSPP1; 40 ng/mL) or neutralizing anti-SPP1 antibody (α-SPP1; 10 μg/mL) followed by cell quantification. Shown are representative fluorescent microscopic images (C) and flow cytometry histograms (D), as well as data summary from *n* = 3 independent experiments (E). *n*, sample size; *columns*, mean; *bars*, SD; *P*, overall probability by one-way ANOVA; * and ***, *P*< 0.05 and *P*< 0.001, respectively, for comparison of the indicated groups with p*GFP*/p*RFP* control co-cultures by Tukey's multiple comparison test; * and ***, *P*< 0.05 and *P*< 0.001, respectively, for comparison of the indicated groups with p*GFP*p*ΔKras*/p*RFP* or p*GFP*/p*RFP*p*ΔKras* co-cultures by Tukey's multiple comparison test. (F-H) *LSL.R26.Luc* mice (*FVB* background; *n* = 8) received a single intraperitoneal injection of urethane (1 g/Kg), were sacrificed after two weeks (when *Kras* mutations occur in the lungs), and single cell suspensions of pulmonary cells were plated (20 000 cells from each mouse/96-well) and incubated for two weeks with PBS control, rmSPP1 (10 ng/mL), or α-SPP1 (10 μg/mL). Cell mass was quantified longitudinally using bioluminescence imaging and after two weeks using cell counting. Shown are representative bioluminescence image (F), as well as data summary from *n* = 8 independent

experiments (G, H). (G) *Circles*, mean; *bars*, SD; *P*, 2-way ANOVA probability; * and ***, $P< 0.05$ and $P< 0.001$, respectively for rmSPP1-treated cells at indicated time-points compared with α-SPP1-treated cells. (H) *circles*, data points; *lines*, median; *boxes*, interquartile range; *bars*, 50% outer quartiles; *P*, overall probability by Kruskal-Wallis test; *, $P< 0.05$ for comparison of the indicated groups with PBS-treated cells by Dunn's post-test.

Figure 6. ***SPP1 drives de novo tumorigenesis in the cellular context of mutant KRAS.*** HEK293T cells were stably transfected with a eukaryotic expression vector encoding *Photinus pyralis* luciferase (p*Cag.Luc*) alone or in combination with mutant murine Kras (p*ΔKras*). Thereafter, pools of 3-5 stable clones were transiently transfected with random sequence control (p*C*) or murine SPP1 (p*Spp1*) plasmids, were validated, and 2 x 10^6 cells expressing p*C* or p*Spp1* were injected pairwise into the rear flanks of *NOD/SCID* mice followed by serial tumor measurements and bioluminescence imaging. (A) Cropped immunoblots of whole cell extracts probed with anti-Kras and anti-α-Tubulin antibodies. (B) SPP1 protein secretion by ELISA. *Circles*, data points; *lines*, median; *boxes*, interquartile range; *bars*, 50% outer quartiles; *P*, Mann-Whitney U-test probability. (C) Legend and schematic representation of experimental set-up. (D) Representative bioluminescence images of living mice at 35 days post-HEK293T cell injection. (E) Numbers of mice used and incidence of tumors larger than 0.3 cm^3. (F) Data summary of tumor volume. (G) Data summary of bioluminescence imaging.(F, G) *Circles*, mean; *bars*, SD; *P*, 2-way ANOVA probability; ns, **, and ***, $P> 0.05$, $P< 0.01$, and $P< 0.001$, respectively for the indicated comparisons at the final time-points. Mice conditionally expressing mutant $KRAS^{G12D}$ upon CRE-mediated recombination (*LSL.*$KRAS^{G12D}$) and simultaneously competent ($Spp1^{+/+}$; *n*=7), haploinsufficient ($Spp1^{+/-}$;*n*=4), or deficient ($Spp1^{-/-}$; *n*=8) in *Spp1* alleles (all on the *C57BL/6* background) received 5 x 10^8 plaque-forming units (PFU) intratracheal adenovirus encoding CRE recombinase (Ad-*Cre*) and were sacrificed 4 months later (I, K). Alternatively,

LSL.KRAS^{G12D} mice were intercrossed with mice conditionally expressing SPP1 upon CRE-mediated recombination (*LSL.SPP1*^{Tg}) and offsprings *LSL.SPP1*^{Tg} (*n*=9), *LSL.KRAS*^{G12D} (*n*=9) and *LSL.KRAS*^{G12D}; *LSL.SPP1*^{Tg} (*n*=9) received 5 x 10^8 PFU Ad-*Cre* and were sacrificed 3 months later (J, L). Shown are experimental schematic with each box representing one month (H), data summary of mouse lung tumor fraction (I, J), as well as hematoxylin and eosin-stained representative lung tissue sections with tumors (K, L, arrows). *n*, sample size; *circles*, data points; *lines*, median; *boxes*, interquartile range; *bars*, 50% outer quartiles; *P*, overall probability by Kruskal-Wallis test; *, $P< 0.05$ for comparison of the indicated group with *LSL.KRAS*^{G12D};*Spp1*$^{+/+}$ mice by Dunn's post-test (b); ***, $P< 0.001$ for comparison of the indicated group with *LSL.SPP1*^{Tg} mice by Dunn's post-test; **, $P< 0.01$ for comparison of the indicated group with *LSL.KRAS*^{G12D} mice by Dunn's post-test.

Figure 1

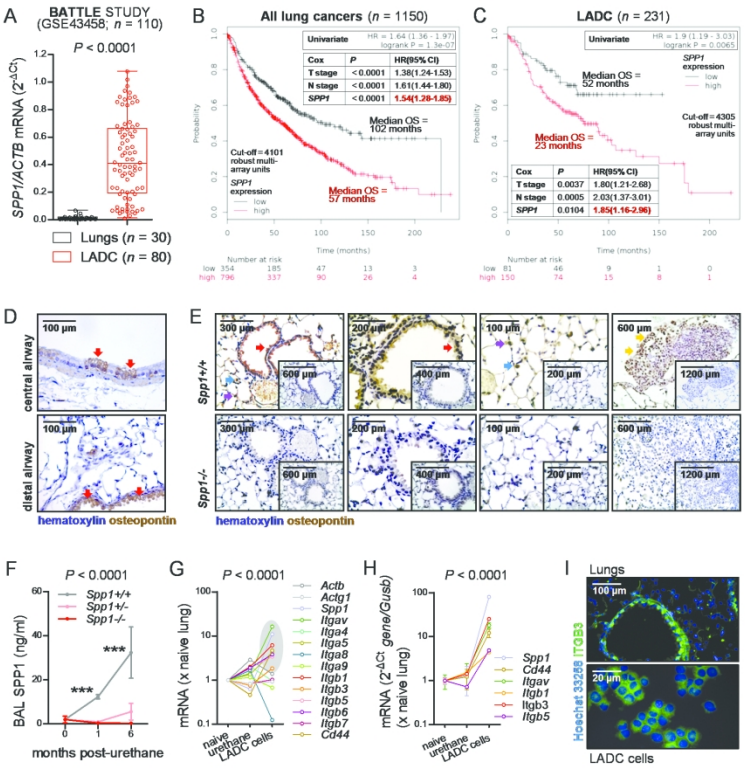

Figure 1. Secreted phosphoprotein 1 (SPP1) is overexpressed in human and murine lung tumors and is associated with poor survival. (A) SPP1 corrected for housekeeping ACTB transcript abundance using the -ΔCT method on microarray data from 30 normal lung and 80 lung adenocarcinoma (LADC) samples from the BATTLE study (GSE43458;[19]). Circles, data points; lines, median; boxes, interquartile range; bars, 50% outer quartiles; n, sample size; P, Mann-Whitney U-test probability. (B, C) Kaplan-Meier and Cox proportional hazards overall survival (OS) analyses of 1150 patients with lung cancer (B) and 231 patients with LADC (C) stratified into low (black) and high (red) SPP1 transcript expression by optimal cut-offs shows that SPP1 overexpression is a stage-independent negative predictor of OS. Lines and numbers, Kaplan-Meier survival plots and risk estimates; P and HR, Univariate Kaplan-Meier and multivariate Cox-regression probabilities (P) and hazard ratios (HR) with 95% confidence intervals (CI); T and N, TNM7 primary tumor and lymph node stage. (D, E) Immunodetection of SPP1 protein (brown) in lungs from naïve C57BL/6 mice (n = 5; d) and from urethane-treated (ten weekly intraperitoneal injections of 1 g/kg; latency 6 months) C57BL/6 mice competent (Spp1+/+; n = 23) or deficient (Spp1-/-; n = 19) in both Spp1 alleles (E) shows high expression by non-ciliated airway epithelial cells (red arrows), alveolar epithelial cells (magenta

arrows), alveolar macrophages (blue arrows), and lung tumor cells (yellow arrows) selectively from Spp1+/+ mice. Inlays, isotype controls. (F) Bronchoalveolar lavage (BAL) SPP1 protein levels from urethane-treated C57BL/6 mice competent (Spp1+/+), haploinsufficient (Spp1+/-), or deficient (Spp1-/-) in Spp1 alleles at 0 (n = 5/group), 1 (n = 7-9/group), and 6 (n = 5-8/group) months post-treatment start shows increased SPP1 elaboration into the airspaces during chemical carcinogenesis. Dots, mean; bars, SD; n, sample size; P, 2-way ANOVA probability; ***, P< 0.001 for Spp1+/+ mice at indicated time-points compared with time-point 0 months. (G, H) Microarray (G) and qPCR (h) results of relative abundance of SPP1 and its receptors' transcripts in RNA extracted from naïve FVB mouse lungs, urethane-exposed FVB mouse lungs at 1 week post 1 g/Kg urethane, and primary LADC cells derived from urethane-induced lung tumors ([22]; GSE94981; g, n= 2/group; h, n = 3/group) identify and validate overexpression of Spp1, Itgav, Itgb1, Itgb3, Itgb5, and Cd44 (grey area) by LADC cells relative to Gusb housekeeping transcript. Dots, mean; bars, SD; n, sample size; P, 2-way ANOVA probability. (I) Representative integrin-β3 (ITGB3) immunoreactivity (green) of naïve murine lungs and primary LADC cells derived from urethane-induced lung tumors (n = 5/group) counterstained with Hoechst 33258 (blue).

190x254mm (300 x 300 DPI)

Figure 2

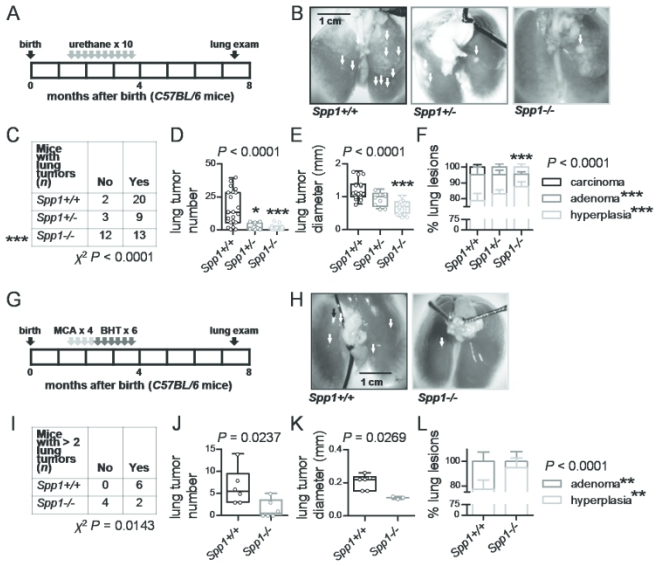

Figure 2. SPP1 promotes chemical-induced lung carcinogenesis. (A-F) Spp1+/+, Spp1+/-, and Spp1-/- mice on the C57BL/6 background were treated with urethane and were sacrificed six months post-urethane start for assessment of pulmonary oncogenesis. Shown are experimental schematic with each box representing one month (A), photographs of representative lungs with tumors (B, arrows), as well as data summary of mouse numbers (n) and tumor incidence (C), number of lung tumors (D), diameter of lung tumors (E), and histologic distribution of neoplastic lesions (F). n, sample size; circles, data points; lines, median; boxes, interquartile range; bars, 50% outer quartiles; P, overall probability by χ2 test (c), Kruskal-Wallis test (D, E), and two-way ANOVA (F); * and ***, P< 0.05 and P< 0.001, respectively, for comparison of the indicated group with Spp1+/+ mice by Fischer's exact test (C), Dunn's multiple comparison test (D, E), and Bonferroni post-test (F). (G-L) Spp1+/+ and Spp1-/- mice on the C57BL/6 background were treated with 3-methylcholanthrene (MCA) followed by butylated hydroxytoluene (BHT) and were sacrificed six months post-MCA start for assessment of pulmonary oncogenesis. Shown are experimental schematic with each box representing one month (G), photographs of representative lungs with tumors (H, arrows), as well as data summary of mouse numbers (n) and tumor incidence (I), number of lung tumors (J), diameter of lung

tumors (K), and histologic distribution of neoplastic lesions (L) according to [50]. n, sample size; circles, data points; lines, median; boxes, interquartile range; bars, 50% outer quartiles; P, overall probability by $\chi 2$ test (I), Mann-Witney U-test (J, K), and two-way ANOVA (L); **, P< 0.01 for comparison of the indicated group with Spp1+/+ mice by Bonferroni post-test (L).

190x254mm (300 x 300 DPI)

Figure 3

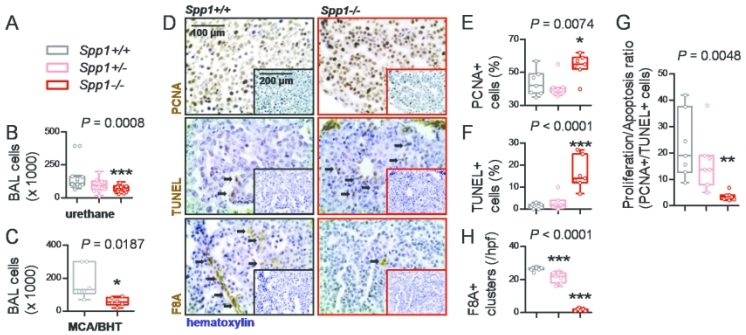

Figure 3. SPP1 fosters inflammation, neovascularization, and cancer cell survival in de novo lung tumors. Spp1+/+, Spp1+/-, and Spp1-/- mice on the C57BL/6 background were treated with urethane or 3-methylcholanthrene (MCA) followed by butylated hydroxytoluene (BHT) and were sacrificed six months post-treatment start as in Figures 2A and 2G, respectively. (A) Legend to experimental groups. Nucleated cell numbers of bronchoalveolar lavage (n = 16, 12, and 25, respectively, for Spp1+/+, Spp1+/-, and Spp1-/- mice treated with urethane (B) and n = 6/group for Spp1+/+ and Spp1-/- mice treated with MCA/BHT, (C). Shown are representative images (D) from the immunoreactivity (brown color; arrows) of lung tumors from urethane-treated mice for proliferating cell nuclear antigen (PCNA, top), terminal deoxynucleotidyl nick-end labeling (TUNEL, middle), and factor VIII-related antigen (F8A, bottom) protein expression (blue color indicates hematoxylin counterstain), and data summary (E-G) from n = 7 mice/group (ten different tumors from each mouse were examined and averaged). Inlays, isotype controls. n, sample size; circles, data points; lines, median; boxes, interquartile range; bars, 50% outer quartiles; P, overall probability, Unpaired t-test (C) and one-way ANOVA with Tuckey's Multiple Comparison Test (B,E-G); *, P< 0.05, **, P< 0.01 and ***and P< 0.001, respectively, for comparison of the indicated group with Spp1+/+ mice by Dunn's

multiple comparison test.

190x254mm (300 x 300 DPI)

Figure 4

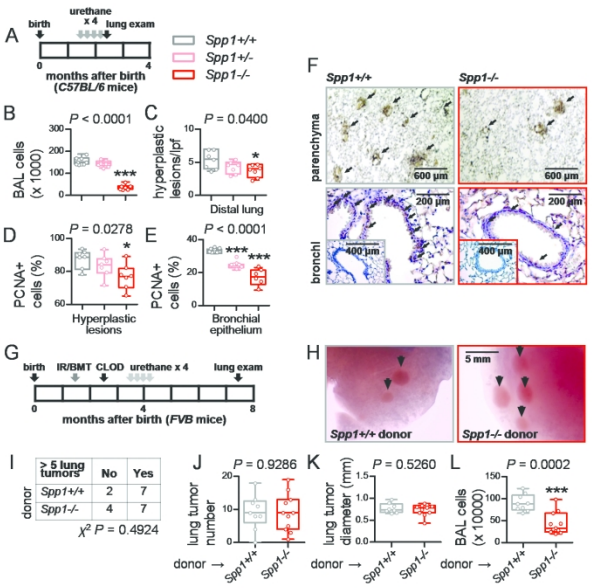

Figure 4. Epithelial-derived SPP1 drives preneoplasia in the tumor-initiated lung. (A-F) Spp1+/+(n = 9), Spp1+/-(n = 9), and Spp1-/-(n = 7) mice on the C57BL/6 background were treated with urethane and were sacrificed one month post-treatment start. Shown are experimental schematic with each box representing one month (A), data summary of nucleated cell numbers of bronchoalveolar lavage (B), number of atypical alveolar hyperplastic lesions (C), proliferating cell nuclear antigen (PCNA) immunoreactive cell abundance within these lesions (D), and PCNA immunoreactive cell abundance in airway epithelium (E), as well as representative images of PCNA immunoreactivity of alveolar (top) and airway (bottom) regions (F). Inlays, isotype controls. n, sample size; circles, data points; lines, median; boxes, interquartile range; bars, 50% outer quartiles; P, overall probability by Kruskal-Wallis test; * and ***, P< 0.05 and P< 0.001, respectively, for comparison of the indicated group with Spp1+/+ mice by Dunn's multiple comparison test. (G-L) FVB mice received total body irradiation (900 Rad, IR) followed by same-day bone marrow transplants (ten million cells flushed from the four long bones; BMT) from Spp1+/+ and Spp1-/- mice. After one month necessary for bone marrow reconstitution, chimeras received intratracheal clodronate aimed at alveolar macrophage depletion and their reconstitution by bone marrow-derived

chimeric macrophages, which is complete after another month [31], when animals received urethane and were sacrificed six months post-urethane start for assessment of pulmonary oncogenesis. Shown are experimental schematic with each box representing one month (G), photographs of representative lungs with tumors (H, arrows), as well as data summary of mouse numbers (n) and tumor incidence (I), number of lung tumors (J), diameter of lung tumors (K), and nucleated cell numbers of bronchoalveolar lavage (L). n, sample size; circles, data points; lines, median; boxes, interquartile range; bars, 50% outer quartiles; P, overall probability by $\chi 2$ test (I) and Mann-Witney U-test (J-L).

190x254mm (300 x 300 DPI)

Figure 5

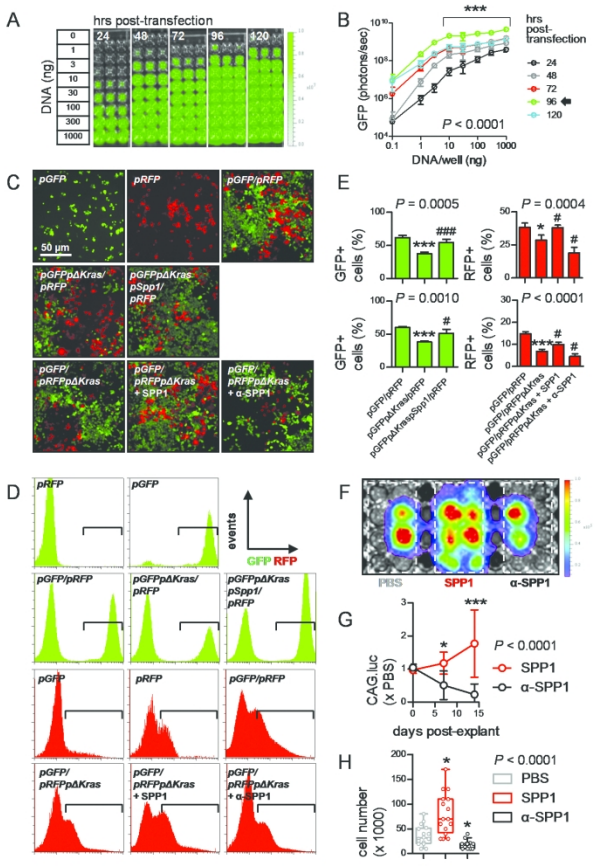

Figure 5. SPP1 fosters the survival of KRAS-mutant cells. (A, B) HEK293T benign human embryonic kidney cells were transiently transfected with varying amounts of a eukaryotic expression vector encoding enhanced GFP and green fluorescence was quantified by serial biofluorescence imaging of live cells. Shown are representative biofluorescence images (A) and summary of data from n = 3 independent experiments (B). Circles, mean; bars, SD; n, sample size; P, 2-way ANOVA probability; ***, P< 0.001 for plasmid amounts ≥ 10 ng/well at 96 hours compared with all other time-points and with 0 ng/well DNA. (C-E) HEK293T cells were stably transfected with eukaryotic expression vectors encoding enhanced GFP (pGFP) or RFP (pRFP). Thereafter, pGFP-expressing cells were transiently transfected with eukaryotic expression vectors encoding mutant murine Kras(pΔKras) alone or pΔKras plus murine SPP1 (pSpp1), were mixed with equal numbers of pRFP-expressing HEK293T cells, co-cultured for one week, and finally were quantified by fluorescent microscopy and flow cytometry. Alternatively, pRFP-expressing cells were transiently transfected with pΔKras, mixed with equal numbers of pGFP-expressing cells, and were co-incubated for one week with recombinant murine SPP1 (rmSPP1; 40 ng/mL) or neutralizing anti-SPP1 antibody (α-SPP1; 10 µg/mL) followed by cell quantification. Shown are representative fluorescent microscopic images (C) and flow

cytometry histograms (D), as well as data summary from n = 3 independent experiments (E). n, sample size; columns, mean; bars, SD; P, overall probability by one-way ANOVA; * and ***, P< 0.05 and P< 0.001, respectively, for comparison of the indicated groups with pGFP/pRFP control co-cultures by Tukey's multiple comparison test; * and ***, P< 0.05 and P< 0.001, respectively, for comparison of the indicated groups with pGFPpΔKras/pRFP or pGFP/pRFPpΔKras co-cultures by Tukey's multiple comparison test. (F-H) LSL.R26.Luc mice (FVB background; n = 8) received a single intraperitoneal injection of urethane (1 g/Kg), were sacrificed after two weeks (when Kras mutations occur in the lungs), and single cell suspensions of pulmonary cells were plated (20 000 cells from each mouse/96-well) and incubated for two weeks with PBS control, rmSPP1 (10 ng/mL), or α-SPP1 (10 μg/mL). Cell mass was quantified longitudinally using bioluminescence imaging and after two weeks using cell counting. Shown are representative bioluminescence image (F), as well as data summary from n = 8 independent experiments (G, H). (G) Circles, mean; bars, SD; P, 2-way ANOVA probability; * and ***, P< 0.05 and P< 0.001, respectively for rmSPP1-treated cells at indicated time-points compared with α-SPP1-treated cells. (H) circles, data points; lines, median; boxes, interquartile range; bars, 50% outer quartiles; P, overall probability by Kruskal-Wallis test; *, P< 0.05 for comparison of the indicated groups with PBS-treated cells by Dunn's post-test.

190x254mm (300 x 300 DPI)

Figure 6

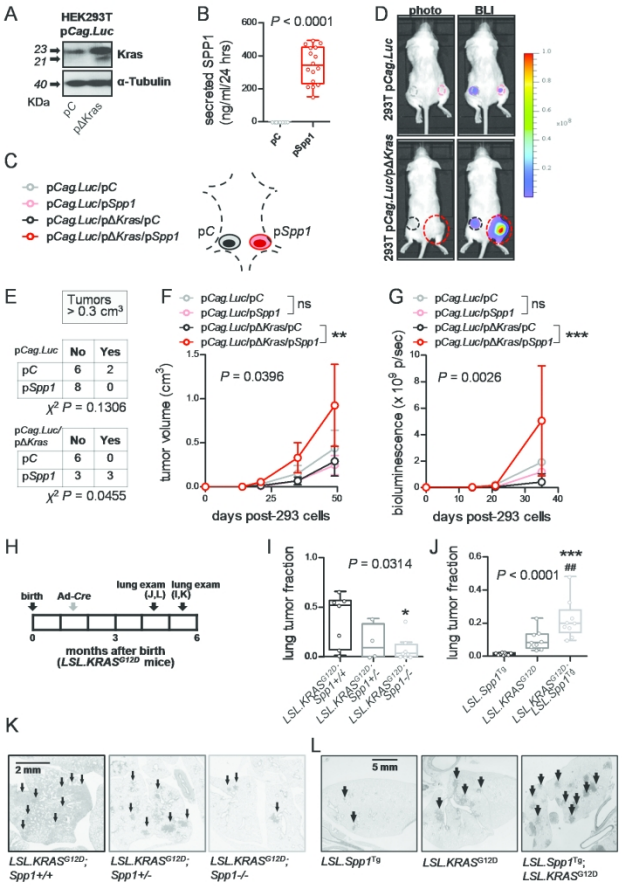

Figure 6. SPP1 drives de novo tumorigenesis in the cellular context of mutant KRAS. HEK293T cells were stably transfected with a eukaryotic expression vector encoding Photinus pyralis luciferase (pCag.Luc) alone or in combination with mutant murine Kras (pΔKras). Thereafter, pools of 3-5 stable clones were transiently transfected with random sequence control (pC) or murine SPP1 (pSpp1) plasmids, were validated, and 2 x 106 cells expressing pC or pSpp1 were injected pairwise into the rear flanks of NOD/SCID mice followed by serial tumor measurements and bioluminescence imaging. (A) Cropped immunoblots of whole cell extracts probed with anti-Kras and anti-α-Tubulin antibodies. (B) SPP1 protein secretion by ELISA. Circles, data points; lines, median; boxes, interquartile range; bars, 50% outer quartiles; P, Mann-Whitney U-test probability. (C) Legend and schematic representation of experimental set-up. (D) Representative bioluminescence images of living mice at 35 days post-HEK293T cell injection. (E) Numbers of mice used and incidence of tumors larger than 0.3 cm3. (F) Data summary of tumor volume. (G) Data summary of bioluminescence imaging.(F, G) Circles, mean; bars, SD; P, 2-way ANOVA probability; ns, **, and ***, P> 0.05, P< 0.01, and P< 0.001, respectively for the indicated comparisons at the final time-points. Mice conditionally expressing mutant KRASG12D upon CRE-mediated recombination (LSL.KRASG12D) and

simultaneously competent (Spp1+/+; n=7), haploinsufficient (Spp1+/-;n=4), or deficient (Spp1-/-; n=8) in Spp1 alleles (all on the C57BL/6 background) received 5 x 108 plaque-forming units (PFU) intratracheal adenovirus encoding CRE recombinase (Ad-Cre) and were sacrificed 4 months later (I, K). Alternatively, LSL.KRASG12D mice were intercrossed with mice conditionally expressing SPP1 upon CRE-mediated recombination (LSL.SPP1Tg) and offsprings LSL.SPP1Tg (n=9), LSL.KRASG12D (n=9) and LSL.KRASG12D; LSL.SPP1Tg (n=9) received 5 x 108 PFU Ad-Cre and were sacrificed 3 months later (J, L). Shown are experimental schematic with each box representing one month (H), data summary of mouse lung tumor fraction (I, J), as well as hematoxylin and eosin-stained representative lung tissue sections with tumors (K, L, arrows). n, sample size; circles, data points; lines, median; boxes, interquartile range; bars, 50% outer quartiles; P, overall probability by Kruskal-Wallis test; *, P< 0.05 for comparison of the indicated group with LSL.KRASG12D;Spp1+/+ mice by Dunn's post-test (b); ***, P< 0.001 for comparison of the indicated group with LSL.SPP1Tg mice by Dunn's post-test; **, P< 0.01 for comparison of the indicated group with LSL.KRASG12D mice by Dunn's post-test.

190x254mm (300 x 300 DPI)

Supplementary Material

Osteopontin drives KRAS-mutant lung adenocarcinoma.

Ioanna Giopanou, Nikolaos I. Kanellakis,Anastasios D. Giannou, Ioannis Lilis, Antonia Marazioti, Magda Spella,Vassilios Papaleonidopoulos, Davina C.M. Simoes, Dimitra E. Zazara, Theodora Agalioti, Charalampos Moschos, Sophia Magkouta, Ioannis Kalomenidis, Vily Panoutsakopoulou, Anne-Sophie Lamort, Georgios T. Stathopoulos, and Ioannis Psallidas

SUPPLEMENTARY METHODS

Assessment of lung inflammation: Bronchoalveolar lavage (BAL) was performed with 3 x1000 µl sterile saline. Fluid was combined and centrifuged (260g, 10 min), cells were resuspended in 1 ml phosphate-buffered saline and 1% bovine serum albumin, total cell counts were determined using a grid hemocytometer[1].

Enzyme-linked immunosorbent assay (ELISA): SPP1 protein levels of Bronchoalveolar lavage (BAL) was determined using dedicated murine ELISA kits according to the manufacturer's instructions (Peprotech, London, UK and R&D Systems, Minneapolis, MN).

qPCR and microarray: RNA was isolated using Trizol (Invitrogen) followed by RNAeasy (QIAGEN), RNA was reverse transcribed using Superscript III (Invitrogen), and reverse transcriptase or qPCR was performed using specific primers (Supplemental Table 2). For microarray, 5 µg RNA pooled from triplicate samples was tested for quality, labeled, and hybridized to GeneChip Mouse Gene 1.0 or 2.0 ST arrays (Affymetrix). Microarray data are available at the GEO database (https://www.ncbi.nlm.nih.gov/geo/) using accession ID GSE94981.

Flow cytometry: Cells were analyzed on a FACS Calibur (BD Biosciences) for endogenous fluorescence. Data were examined using FlowJo (Ashland, OR).

Immunoblotting: Whole cell extracts were prepared using RIPA buffer (Sigma Aldrich, (St Louis, MO), separated by 10% SDS-PAGE, and electroblotted to PVDF membranes (Merck-Millipore, Darmstadt, Germany). Membranes were labeled using the indicated antibodies (Supplemental Table 3) followed by incubation with the appropriate HRP-conjugated secondary antibodies at the manufacturers' indicated dilutions and were visualized using enhanced chemiluminescence substrate (Merck Millipore, Darmstadt, Germany).

Histology and Cytology: Lungs were exsanguinated, inflated at 20 cmH_2O with 10% neutral-buffered formalin, and fixed overnight. Lung tumor number and diameter (δ) were measured under a Stemi DV4 stereoscope (Zeiss; Jena, Germany) and tumor volume (V) was calculated as $\pi\delta^3/6$ and averaged/summed. Lung volume was measured by saline immersion, lungs were embedded in paraffin. Lungs were fixed in 10% paraffin or in 4% paraformaldehyde overnight, were embedded in paraffin or in optimal cutting temperature (OCT; Sakura, Tokyo, Japan) and were stored at room temperature or -80^o C, respectively, till further analyses. Five-µm paraffin or 10-µm-cryosections were mounted on glass slides. Sections were mounted on glass slides and stained with hematoxylin and eosin (H&E). The proportion (percent of total lung lesions) consisting of each type of distinct lung lesions, including atypical alveolar hyperplasia (AAH), adenoma (AD), and adenocarcinoma (AC), on the sections from each lung were evaluated by two blinded readers (IP and GTS). Lung tumor burden was determined by point counting of the ratio of the area occupied by tumor versus the lung area and by extrapolating the average ratio per mouse to total lung volume, as described elsewhere[3]. Alternatively, tissue sections were immune-labeled with specific antibodies against SPP1, PCNA, factor VIII-related antigen (fVIIIra) and TUNEL as described previously[4]. The number of immunoreactive cells in lungs (bronchial and alveolar epithelium) and lung tumors was evaluated by two blinded readers in at least five high-power visual fields of at least five different lung or tumor regions per lung. The results were averaged per mouse. Sections were labeled using the indicated antibodies (Supplemental Table 3) and detected by Envision/diaminobenzidine detection (Dako, Glostrup, Denmark) kit or counterstained with hematoxylin/eosin working solution or with Hoechst 33258 (Sigma-Aldrich) and were mounted with Entellan new (Merck Millipore, Darmstadt,

Germany) or with Mowiol 4-88 (Calbiochem, Gibbstown, NJ). A 100-point-grid was superimposed on ≥ 5 random non-overlapping fields of ≥ 10 sections/lung using Fiji and lung tumor burden was determined by extrapolating tumor-to-lung point counts to lung volume[3]. For isotype control, primary antibody was omitted. Bright-field images were captured with an AxioLab.A1 microscope connected to an AxioCam ERc 5s camera (Zeiss, Jena, Germany). Fluorescent microscopy was carried out on an AxioObserver.D1 inverted (Zeiss) or a TCS SP5 confocal microscope (Leica MS-20 Microsystems, Heidelberg, Germany) and digital images were processed with Fiji software[5].

SUPPLEMENTARY REFERENCES

1. Kourepini E, Aggelakopoulou M, Alissafi T, Paschalidis N, Simoes DC, Panoutsakopoulou V. Osteopontin expression by CD103- dendritic cells drives intestinal inflammation. Proc NatlAcadSci U S A 2014; 111: E856-865.

2. Giopanou I, Lilis I, Papaleonidopoulos V, Agalioti T, Kanellakis NI, Spiropoulou N, Spella M, Stathopoulos GT. Tumor-derived osteopontin isoforms cooperate with TRP53 and CCL2 to promote lung metastasis. Oncoimmunology 2017; 6: e1256528.

3. Hsia CC, Hyde DM, Ochs M, Weibel ER. An official research policy statement of the American Thoracic Society/European Respiratory Society: standards for quantitative assessment of lung structure. Am J RespirCrit Care Med 2010; 181: 394-418.

4. Darzynkiewicz Z, Galkowski D, Zhao H. Analysis of apoptosis by cytometry using TUNEL assay. Methods 2008; 44: 250-254.

5. Schindelin J, Arganda-Carreras I, Frise E, Kaynig V, Longair M, Pietzsch T, Preibisch S, Rueden C, Saalfeld S, Schmid B, Tinevez JY, White DJ, Hartenstein V, Eliceiri K, Tomancak P, Cardona A. Fiji: an open-source platform for biological-image analysis. Nat Methods 2012; 9: 676-682.

SUPPLEMENTARY TABLES

Supplementary Table 1. Number of experimental mice (*n*) used for these studies.

	Strain designation	**Jackson Laboratory Stock #**	**Short strain designation**	***n***
Parental strains	*C57BL/6J*	000664	*C57BL/6*	67
	B6.129S6-*Spp1*^{tm1Blh}*/J*	004936	*Spp1*$^{-/-}$	59
	FVB/NJ	001800	*FVB*	30
	B6.129S4-*Kras*^{tm4Tyj}*/J*	008179	*LSL.KRAS*^{G12D}	16
	FVB-Tg$^{(CAG\text{-}luc,\text{-}GFP)L2G85Chco}$*/J*	008450	*CAG-luc-eGFP*	8
	NOD.CB17-*Prkdc*$^{<scid>}$*/J*	001303	*NOD/SCID*	14
	Spp1-stop$^{f/f}$*/CreER*^{T1}	-	*LSL.Spp1*^{Tg}	9
Inter-crosses	-	-	*SPP1*$^{+/-}$	40
	-	-	*LSL.KRAS*^{G12D}*;Spp1*$^{+/-}$	4
	-	-	*LSL.KRAS*^{G12D}*;Spp1*$^{-/-}$	8
	-	-	*LSL.KRAS*^{G12D}*;LSL.Spp1*^{Tg}	9
			Total	**264**

Supplementary Table 2. PCR primers used for these studies.

Method[a]	Primer	Sequence
qPCR	mSpp1F	CCCTTTCCGTTGTTGTCCTG
	mSpp1R	GATGAACAGTATCCTGATGCCAC
	CD44F	CGTCCAACACCTCCCACTAT
	CD44R	TGGTAACCGGTCCATCGAAG
	GusbvF	TTACTTTAAGACGCTGATCACC
	GusbR	ACCTCCAAATGCCCATAG
	ItgavF	TGGCTATTCAATGAAGGGAG
	ItgavR	AGGGTACACTTCAAGGCCAG
	Itgb1F	TCCAGCTAATCATCGATGCCT
	Itgb1R	TTCTCCTGTCCCATTCACC
	Itgb3F	CTGGCAAGTACTGTGAGTGC
	Itgb3R	AGTAGTAGCCAGTCCAGTCC
	Itgb5F	ACCGAGATACCAGACCAATCC
	Itgb5R	CCTCTGCTTCCTCACTTCCT
PCR	MycoplasmaF	GGGAGCAAACAGGATTAGATACCCT
	MycoplasmaR	TGCACCATCTGTCACTCTGTTAACCTC
	mSpp1F (*LSL.Spp1*^{Tg})	CTGCTAGTACACAAGCAGAC
	mSpp1R (*LSL.Spp1*^{Tg})	GCCTCTTCTTTAGTTGACCTC
	mSpp1F1	CCATACAGGAAAGAGAGACC
	mSpp1F2	CGTCCTGTAAGTCTGCAGAA
	mSpp1R	AACTGTTTTGCTTGCATGCG

[a] Application: qPCR, quantitative real-time polymerase chain reaction; PCR, polymerase chain reaction.

Supplementary Table 3. Antibodies used in these studies.

Method[a]	Target	Provider[b]	Catalog#	Dilution	Conjugate[c]
WB	KRAS2A	Santa Cruz	sc-522	1:200	-
	α-Tubulin	Sigma	T5168	1:4000	-
	Goat anti-mouse IgG	Southern Biotech	1030-05	1:8000	HRP
	Goat anti-rabbit IgG	Southern Biotech	4030-05	1:8000	HRP
IHC/IF	SPP1	Abcam	ab91655	1:1000	-
	PCNA	Abcam	ab2426	1:2000	-
	F8A	Invitrogen	PA5-61382	1:1000	-
	ITGB3	Sigma-Aldrich	SAB4501586	1:1000	-
	donkey anti-rabbit & anti-mouse IgG	Invitrogen	A21206 - A21202	1:1000	Alexa 488

[a]Application: WIB, Western immunoblotting; IF, immunofluorescence; IHC, immunochistochemistry; [b]Providers: Santa Cruz Biotechnology, San Diego, CA; Sigma Aldrich, Taufkirchen, Germany; Abcam, Cambridge, UK; Southern Biotech, Birmingham, AL; Invitrogen, Carlsbad, CA. [c]Conjugates: HRP, horse radish peroxidase.

Supplementary Figure 1. Uncropped gells from the electrophoresis shown in Figure 6A of the manuscript.

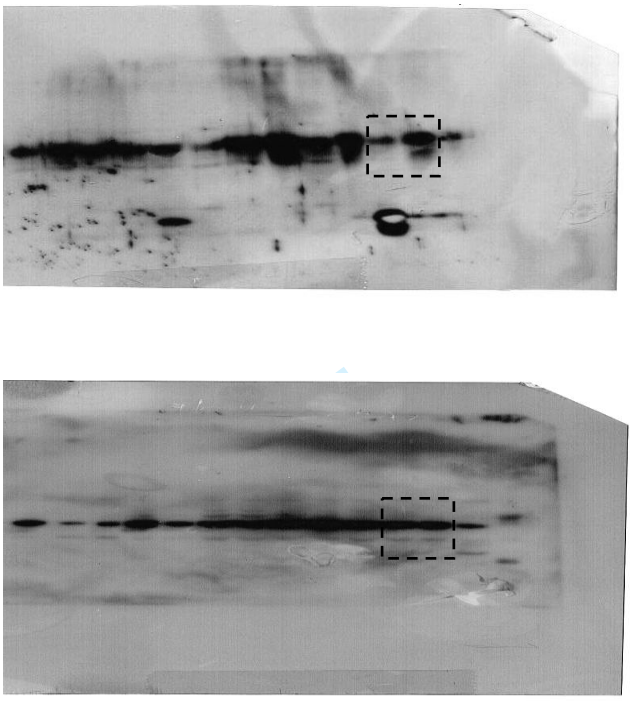

Supplementary Figure 2: Validation of SPP1 expression in *LSL.Spp1*^{Tg}, *LSL.KRAS*^{G12D}, and *LSL.KRAS*^{G12D}; *LSLSpp1*^{Tg} mice upon Ad-*Cre* administration as shown in Figure 6J.